J Mater Sci (2016) 51:3170–3181
DOI 10.1007/s10853-015-9627-3

Multifunctional magnetic branched polyethylenimine nanogels with in-situ generated Fe_3O_4 and their applications as dye adsorbent and catalyst support

Xin Wen[1,2] · Xianliang Qiao[1] · Xue Han[1] · Libo Niu[1] · Li Huo[1] · Guoyi Bai[1]

Received: 11 October 2015 / Accepted: 26 November 2015 / Published online: 21 December 2015

Abstract A series of novel magnetic branched polyethylenimine nanogels (Fe_3O_4/bPEI) was prepared via the combination of crosslinking branched polyethylenimine to form a nanogel and in-situ generation of Fe_3O_4 on its surface. Morphologies and magnetic properties of the Fe_3O_4/bPEI nanocomposites could be easily controlled by regulating the ratio between branched polyethylenimine nanogel and Fe_3O_4 precursor. The nanocomposites could be applied as efficient and selective dye adsorbents for the removal of Congo red under different pH values or in the presence of methylene blue. Furthermore, it could also be applied as catalyst support for the loading of palladium to afford a novel Pd-Fe_3O_4/bPEI nanocomposite, which exhibited good catalytic activity in the reduction of nitrophenols using $NaBH_4$ as the reducing agent. Particularly, this nanocomposite could be easily separated by an external magnetic field and recycled ten times without appreciable loss of its initial catalytic activity. The synergistic integration of nanogel and magnetic Fe_3O_4 nanoparticles makes Fe_3O_4/bPEI to be a versatile platform for multiple applications.

Graphical Abstract Magnetically recyclable polyethylenimine nanogels (Fe_3O_4/bPEI), prepared with in-situ generated Fe_3O_4, can serve as excellent dye adsorbent and catalyst support.

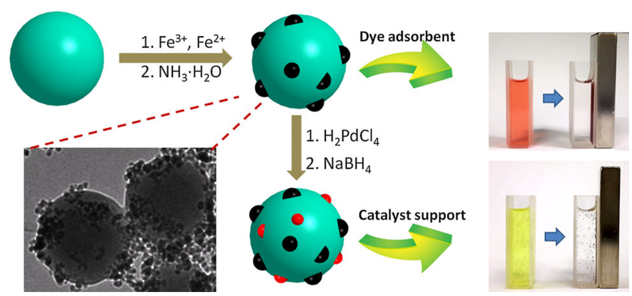

Introduction

Polymeric micro/nanogels have attracted much attention in recent years not only due to their unique physicochemical properties, including small size, large surface areas, tunable dimensions, stable interior network structures, and short response times, but also due to their wide applications in adsorption, catalysis, biosensor, bioimaging, and drug delivery [1–8]. Particularly, within the field of adsorption and catalysis, micro/nanogels have aroused considerable interest due to their multiple accessible channels for the diffusion and transport of guest molecules or ions [9–12], as well as their unimolecular polymeric small-sized entities for retaining their form under a range of catalytic conditions [13–16].

Branched polyethylenimine (bPEI), as one of the most important water-soluble cationic polymers, is an attractive

Electronic supplementary material The online version of this article (doi:10.1007/s10853-015-9627-3) contains supplementary material, which is available to authorized users.

✉ Guoyi Bai
baiguoyi@hotmail.com

1 Key Laboratory of Chemical Biology of Hebei Province, College of Chemistry and Environmental Science, Hebei University, Baoding 071002, Hebei, People's Republic of China

2 Hebei Chemical and Pharmaceutical College, Shijiazhuang 050026, Hebei, People's Republic of China

adsorbing and supporting material due to its unique structure and properties. It possesses a large number of amino groups in the backbone and terminals, which endow it certain amino-induced applications, such as being employed as dye [17], metal ion [18] or carbon dioxide adsorbent [19], catalyst support [20], as well as dye-fixing agent in the textile industry [21]. Undoubtedly, bPEI nanogel would be a perfect substrate to adsorb guest ions or molecules. The electron-rich feature of amino groups on the surface and in the network of bPEI nanogel makes it active in the complexation with metal ion [22, 23]. On the other hand, the high positive charge density on the surface of bPEI nanogel facilitates the adsorption of anionic molecules by its polymer network [22, 24]. However, the general methods to separate traditional polymeric nanogels from solutions are through filtration and centrifugation, which are tedious and time-consuming processes. In addition, these methods are not sufficient enough to completely remove nanogels from solutions, limiting the actual applications of polymeric nanogels.

As is well known, magnetic separation provides a quick, simple, eco-friendly, and effective method for the recycling of nanomaterials [25–27]. Accordingly, it might be a good choice to separate polymeric nanocomposites. Until now, two strategies have been developed to construct magnetic polymeric nanocomposites [28–31]. The first strategy combines a surface modification of Fe_3O_4 nanoparticles (NPs) and a subsequent radical polymerization on its surface. For instance, some core–shell magnetic nanocomposites, such as Fe_3O_4@poly(methyl methacrylate) [32], Fe_3O_4@poly(*N*,*N*-methylenebisacrylamide-*co*-methacrylic acid) [33], and Fe_3O_4@poly(4-vinylpyridine-*co*-divinylbenzene) [34], have been prepared by the double-bond-functionalization on the surface of Fe_3O_4 NPs and the subsequent radical polymerization in the presence of required monomer and crosslinking agent. However, surface modification is often prohibitively time-consuming, and has some drawbacks such as high preparation cost and deterioration of the magnetic properties. The second strategy is based on the oxidative polymerization of certain monomers, such as aniline [35], dopamine [36], and pyrrole [37], on the surface of bare Fe_3O_4 NPs. Obviously, both of the current strategies require a robust and effective polymerization. To the best of our knowledge, there is no report on the preparation of magnetic polymer Fe_3O_4 hybrid nanogels with well-defined nanostructures via a condensation reaction.

In this work, we have developed a facile method for the preparation of novel hybrid multifunctional magnetic branched polyethylenimine nanocomposites (Fe_3O_4/bPEI) with in-situ generated Fe_3O_4 NPs. The influence of the ratio between bPEI nanogel and Fe_3O_4 precursor on the morphologies and magnetic properties was systematically studied based on necessary characterizations. The nanocomposites could be easily recovered from the aqueous mixture by an external magnetic field. The as-prepared Fe_3O_4/bPEI nanocomposites could be used as high-efficiency and selective adsorbents for the removal of Congo red (CR), an anionic dye. Furthermore, a Pd NPs-immobilized Fe_3O_4/bPEI nanocomposite exhibited excellent catalytic activity in the reduction of nitrophenols in the presence of $NaBH_4$. Particularly, this catalyst can be recycled for 10 successive cycles in the reduction of 4-nitrophenol (4-NP) without appreciable loss of its initial catalytic activity.

Experimental

Materials

bPEI (Mn = 10^4 g mol^{-1}, $M_w/M_n = 2.5$) was purchased from Sigma-Aldrich. 1,2-Dibromoethane (DBE), CR, methylene blue (MB), 2-nitrophenol (2-NP), 3-nitrophenol (3-NP), and 4-NP were purchased from Aladdin Industrial Inc., Shanghai, China. Palladium chloride ($PdCl_2$) was purchased from Tianjin Kemiou Chemical Reagent Co., Ltd., China. Ferric chloride hexahydrate ($FeCl_3·6H_2O$), ferrous chloride tetrahydrate ($FeCl_2·4H_2O$), and sodium borohydride ($NaBH_4$) were purchased from Tianjin Fuchen Chemical Reagents Factory, China.

Preparation of bPEI nanogel

The bPEI nanogel was synthesized by crosslinking of bPEI with DBE via a condensation reaction (Scheme 1), similar to the method reported in the literature [22]. In brief, to a solution (300 mL) of *N*,*N*-dimethylformamide (DMF) containing bPEI (0.8 g), 3 mL of DBE was added. This solution was vigorously stirred at 60 °C for 14 h, and the clear solution gradually changed to a milk-white suspension. Subsequently, the reaction mixture was heated to 80 °C and kept for another 1.5 h to enhance the extent of condensation reaction, with its color turning from milk-white to faint yellow. After cooling down, the bPEI nanogel was cleaned via two cycles of centrifugation (10000 rpm) and water washing (20 mL). Finally, the bPEI nanogel was dispersed in 80 mL of water (9.5 g L^{-1}).

Preparation of Fe_3O_4/bPEI nanocomposites

Magnetic Fe_3O_4/bPEI nanocomposites were prepared via the in-situ formation of Fe_3O_4 NPs on the surface of bPEI nanogel (Scheme 1). In a typical run, $FeCl_3·6H_2O$ (1.0 g, 3.7 mmol) and $FeCl_2·4H_2O$ (0.368 g, 1.85 mmol) were first dissolved in boiled deionized water (30 mL). Certain

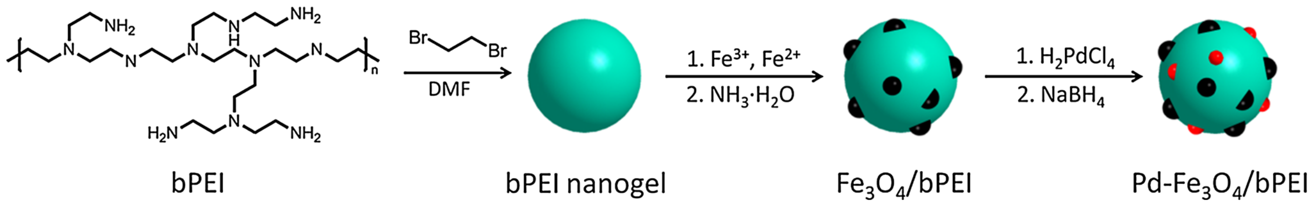

Scheme 1 Schematic illustration of the preparation of Fe_3O_4/bPEI and Pd-Fe_3O_4/bPEI nanocomposites

volume (1.0, 2.0, 4.0, or 8.0 mL) of the above solution was added to the suspension of bPEI nanogel (5.0 mL), and then stirred for 2 h at room temperature for the adsorption of Fe^{3+} and Fe^{2+} ions in the solution. After this mixture was heated to 80 °C, 0.5 mL of $NH_3{\cdot}H_2O$ (25 wt% in water) was injected under vigorous stirring. The color of the mixture turned to black immediately, indicating the formation of the Fe_3O_4 NPs. The as-prepared magnetic Fe_3O_4/bPEI nanocomposites were easily separated from the reaction mixture by magnetic decantation using a permanent magnet and purified by water (10 mL) three times. The Fe_3O_4/bPEI nanocomposites so obtained are denoted as $Fe_3O_{4(1)}$/bPEI, $Fe_3O_{4(2)}$/bPEI, $Fe_3O_{4(4)}$/bPEI, and $Fe_3O_{4(8)}$/bPEI, in which the figure in the parentheses refers to the volume of the Fe^{2+} and Fe^{3+} precursor solution. Finally, the Fe_3O_4/bPEI nanocomposites were dried at 60 °C under vacuum overnight (their final weights were 63.3, 81.0, 111.4, and 164.5 mg, respectively) and then dispersed in 5 mL of water. The preparation conditions of the Fe_3O_4/bPEI nanocomposites and the concentration of the resulting Fe_3O_4/bPEI suspension are summarized in Table 1.

Comparative experiment

A mixture of bPEI nanogel and Fe_3O_4 NPs was prepared by a stepwise procedure. First, Fe_3O_4 NPs were prepared using the same method as that of $Fe_3O_{4(2)}$/bPEI, in which water was used instead of bPEI nanogel suspension. After separated using a magnet, the resulting Fe_3O_4 NPs were added to the bPEI nanogel suspension (5 mL). The mixture was stirred for 2 h at room temperature, followed by centrifugation, dried at 60 °C under vacuum overnight, and denoted as $Fe_3O_{4(2)}$-bPEI (Table 1).

Preparation of Pd-Fe_3O_4/bPEI nanocomposites

First, an aqueous solution of H_2PdCl_4 (0.01 M) was prepared by completely dissolving 44.5 mg of $PdCl_2$ in 25 ml of 20 mM HCl in a boiling water bath [38]. Then, 0.4 mL of H_2PdCl_4 and 1.6 mL of water were successively added into 1.0 mL of $Fe_3O_{4(2)}$/bPEI suspension at room temperature. After 2 h of stirring, a stable mixture was obtained. 50 μL of fresh $NaBH_4$ solution (1.0 M) was then injected into this mixture and kept at room temperature for 2 h. The as-prepared Pd-Fe_3O_4/bPEI nanocomposite was separated by magnetic decantation, washed with water, and finally dispersed in 2 mL of water.

Dye adsorption

The adsorption of different dyes (CR and MB) on Fe_3O_4/bPEI was performed in 100 mL round flasks equipped with a magnetic stirrer at room temperature. 0.1 mL of Fe_3O_4/bPEI suspension was added to a dye solution (40 mL, 80 mg L^{-1}) under different pH values. Over a certain period of time, 3 mL of sample was first removed from the mixture, and then the adsorbent was separated by a permanent magnet. The residual dye concentration in the solution was immediately analyzed by UV–vis measurements to monitor the adsorption process.

Catalytic activity test

The as-prepared Pd-Fe_3O_4/bPEI was used as catalyst for the catalytic reduction of nitrophenols in the presence of $NaBH_4$. In a typical run, 20 μL of Pd-Fe_3O_4/bPEI suspension was first diluted by 2.0 mL of water in a

Table 1 Preparation conditions of the Fe_3O_4/bPEI nanocomposites and the concentration of the resulting Fe_3O_4/bPEI suspension

Sample	Preparation conditions			Concentration (g L^{-1})
	Fe^{2+} and Fe^{3+} (mL)	bPEI nanogel (mL)	$NH_3{\cdot}H_2O$ (mL)	
bPEI nanogel	–	–	–	9.5
$Fe_3O_{4(1)}$/bPEI	1	5	0.5	12.7
$Fe_3O_{4(2)}$/bPEI	2	5	0.5	16.2
$Fe_3O_{4(4)}$/bPEI	4	5	0.5	22.3
$Fe_3O_{4(8)}$/bPEI	8	5	0.5	32.9
$Fe_3O_{4(2)}$-bPEI	2	5	0.5	–

10*10 mm quartz cell. Then, 0.1 mL of nitrophenols solution (2.5 mM) and 0.4 mL of fresh $NaBH_4$ solution (100 mM) were added to the diluted Pd-Fe_3O_4/bPEI solution. The UV–vis adsorption spectra of nitrophenols at different intervals were recorded to monitor the progress of catalytic reaction. When the reaction was complete, the catalysts were magnetically separated from the reaction mixture. After being washed with water, a new portion of aqueous 4-NP and $NaBH_4$ was added for the next cycle of reaction.

Characterization

Inductively coupled plasma-mass spectroscopy (ICP-MS) measurement was performed on an Agilent 7700 spectrometer. X-ray diffraction (XRD) patterns were acquired on a Bruker D8-ADVANCE X-ray diffractometer using Cu Ka radiation and a scan step of 0.02° at 25 °C. X-ray photoelectron spectroscopy (XPS) analysis was carried out on a PHI 1600 spectrometer using Mg Kα X-ray source for excitation. Fourier transform infrared spectroscopy (FTIR) was tested on a Varian-640 spectrophotometer (KBr pellet technique). Thermogravimetric analysis (TGA) was performed on a Perkin-Elmer Pyris 6 type thermogravimetric analyzer under a nitrogen atmosphere (20 mL min^{-1}) at a heating rate of 10 °C min^{-1}. The samples were first pretreated at 100 °C for 30 min to exclude the influence of moisture. Transmission electron microscopy (TEM) images were obtained with a FEI Tecnai G2 F20 S-TWIN instrument at a voltage of 200 kV. Before measurements, the samples were first deposited on a carbon-coated copper grid (200 mesh) and dried at 60 °C for 4 h. Magnetization curves were obtained on a LDJ9600-1 Superconducting quantum interference device. UV–vis spectra were recorded on a Shimadzu WV-2550 spectrophotometer with a slit width of 2 nm and at a scan rate of 600 nm min^{-1}.

Result and discussion

Preparation and characterization of Fe_3O_4/bPEI nanocomposites

The solution of Fe^{3+} and Fe^{2+} was used as the Fe_3O_4 precursor to prepare magnetic Fe_3O_4/bPEI nanocomposites (Scheme 1). During the preparation of Fe_3O_4/bPEI nanocomposites, the adsorption of Fe^{3+} and Fe^{2+} ions by bPEI nanogel is regarded as an important process. To confirm this process, ICP-MS was used to identify the concentration of Fe in the solution before and after adsorption during the $Fe_3O_{4(2)}$/bPEI preparation. It was found that the original Fe concentration was 2.711 g L^{-1} and it decreased to 2.632 g L^{-1} after adsorption. Thus, 2.9 % Fe in the solution was adsorbed by bPEI nanogel during this process. With the addition of $NH_3{\cdot}H_2O$, the adsorbed Fe might act as a seed during the in-situ generation of Fe_3O_4 NPs on the surface of bPEI nanogel [39, 40], benefiting for their formation. For comparison, if $Fe_3O_{4(2)}$/bPEI was prepared without the Fe ions adsorption process, some bPEI nanogel cannot assemble with Fe_3O_4 NPs, resulting in an incomplete separation of bPEI nanogel by a magnet (Fig. S1). Therefore, we can conclude that such a Fe ions adsorption process played a key role in the in-situ generation of Fe_3O_4 NPs on the surface of bPEI nanogel.

XRD patterns of bPEI nanogel, Fe_3O_4, and Fe_3O_4/bPEI nanocomposites are shown in Fig. 1a. As can be seen, bPEI nanogel exhibited only one broad peak at about $2\theta = 25°$ (Fig. 1a, curve 1). In contrast, all Fe_3O_4/bPEI nanocomposites showed characteristic diffraction peaks at about 30.3°, 35.7°, 43.2°, 53.5°, 57.0°, and 62.8° (Fig. 1a, curve 2-5), originated from the (220), (311), (400), (422), (511), and (440) planes of crystal Fe_3O_4 NPs [41]. These peaks matched well with those of pure Fe_3O_4 (Fig. 1a, curve 6, JCPDS: 74-748), demonstrating the formation of Fe_3O_4 NPs. The high-resolution XPS spectrum of Fe 2p in

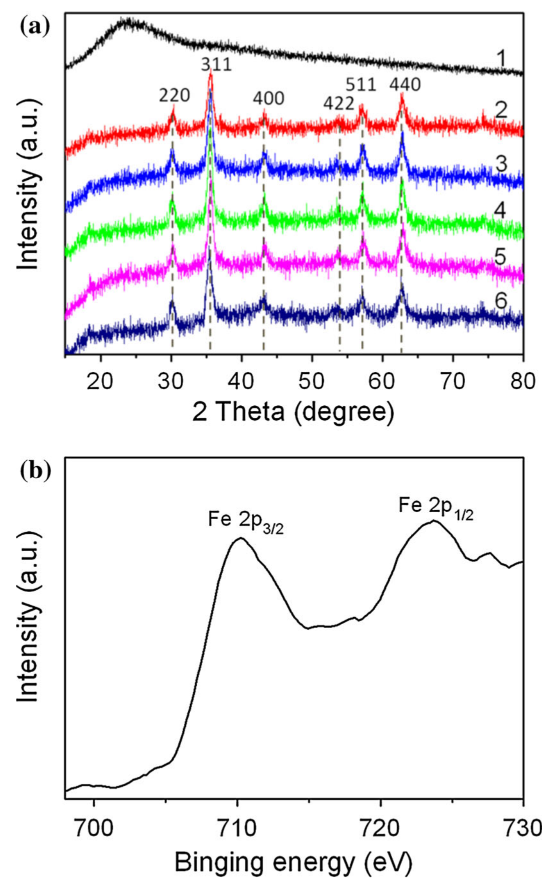

Fig. 1 **a** XRD patterns of (*1*) bPEI nanogel, (*2*) $Fe_3O_{4(1)}$/bPEI, (*3*) $Fe_3O_{4(2)}$/bPEI, (*4*) $Fe_3O_{4(4)}$/bPEI, (*5*) $Fe_3O_{4(8)}$/bPEI, and (*6*) Fe_3O_4. **b** High-resolution XPS spectrum of Fe 2p in $Fe_3O_{4(2)}$/bPEI

$Fe_3O_{4(2)}$/bPEI also supported the formation of Fe_3O_4 (Fig. 1b). The peaks at 710 eV and 724 eV are characteristic of Fe $2p_{3/2}$ and Fe $2p_{1/2}$ in Fe_3O_4, respectively [39]. Combining the results of XRD and XPS, the in-situ formation of Fe_3O_4 in Fe_3O_4/bPEI nanocomposites was well demonstrated.

FTIR spectra of bPEI nanogel, Fe_3O_4/bPEI nanocomposites, and Fe_3O_4, are depicted in Fig. 2a. In the FTIR spectrum of bPEI nanogel (Fig. 2a, curve 1), the characteristic absorption bands at about 3440 and 1654 cm^{-1} were assigned to the stretching vibration of $-NH_2$ and scissor bending vibration of $-NH_2$ [42], and the characteristic absorption bands at 2958–2832 and 1459 cm^{-1} were assigned to the stretching and rocking vibration of C-H, respectively. However, in the spectra of Fe_3O_4/bPEI nanocomposites (Fig. 2a, curve 2-5), all these characteristic absorption bands of bPEI nanogel weakened gradually from $Fe_3O_{4(1)}$/bPEI to $Fe_3O_{4(8)}$/bPEI, whereas an absorption band became stronger at about 580 cm^{-1}, which was assigned to Fe_3O_4 (Fig. 2a, curve 6), suggesting that the content of Fe_3O_4 in the Fe_3O_4/bPEI nanocomposites increased with the decrease of feed ratio between bPEI nanogel and Fe_3O_4 precursor. Subsequently, TGA analysis was carried out to determine the content of Fe_3O_4 in the Fe_3O_4/bPEI nanocomposites based on the residual weight at 750 °C (Fig. 2b). Accordingly, the contents of Fe_3O_4 in $Fe_3O_{4(1)}$/bPEI, $Fe_3O_{4(2)}$/bPEI, $Fe_3O_{4(4)}$/bPEI, and $Fe_3O_{4(8)}$/bPEI were calculated to be 26.3, 40.5, 53.3, and 71.9 %, respectively, indicating that the content of Fe_3O_4 could be controlled by adjusting the ratio between bPEI nanogel and Fe_3O_4 precursor.

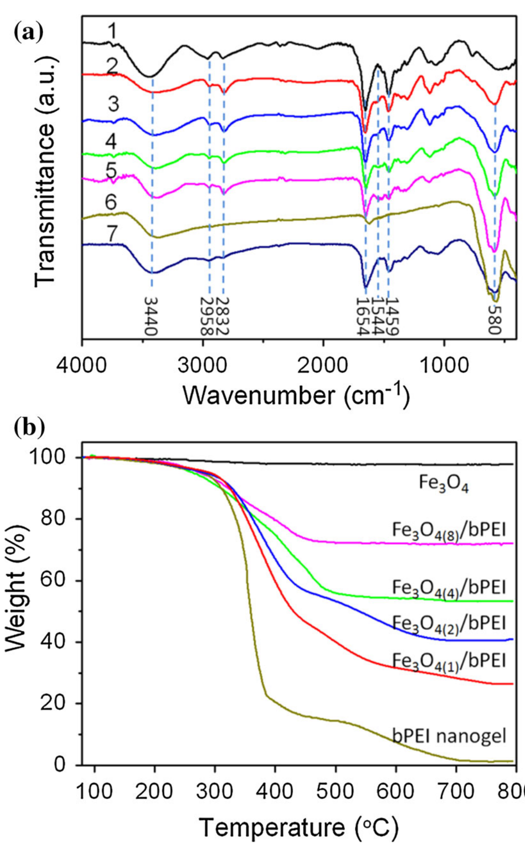

Fig. 2 **a** FTIR spectra of *(1)* bPEI nanogel, *(2)* $Fe_3O_{4(1)}$/bPEI, *(3)* $Fe_3O_{4(2)}$/bPEI, *(4)* $Fe_3O_{4(4)}$/bPEI, *(5)* $Fe_3O_{4(8)}$/bPEI, *(6)* Fe_3O_4, and *(7)* $Fe_3O_{4(2)}$-bPEI. **b** TGA curves of Fe_3O_4, Fe_3O_4/bPEI nanocomposites and bPEI nanogel

Notably, a new characteristic absorption band occurred at about 1544 cm^{-1} in the Fe_3O_4/bPEI nanocomposites and its intensity also increased with the decrease of the ratio between bPEI nanogel and Fe_3O_4 precursor (Fig. 2a, curve 2–5). In contrast, there was no band in this location in the spectrum of $Fe_3O_{4(2)}$-bPEI (Fig. 2a, curve 7). Furthermore, Fe_3O_4 NPs and bPEI nanogel in $Fe_3O_{4(2)}$-bPEI were independent of each other, and the bPEI nanogel in $Fe_3O_{4(2)}$-bPEI cannot be separated by a magnet (Fig. S2), indicating that Fe_3O_4 could not self-assemble to bPEI nanogel by the stepwise procedure adopted in the comparative experiment. Moreover, to eliminate the suspicion of bPEI hydrochloride, formed between bPEI nanogel and H^+ in the Fe^{3+} and Fe^{2+} solution, FTIR measurement of bPEI hydrochloride nanogel was carried out and no band was detected at around 1544 cm^{-1} (Fig. S3). Thus, this new band can be attributed to the assembly of bPEI nanogel and Fe_3O_4 NPs, demonstrating the in-situ formation of Fe_3O_4 on the surface of bPEI nanogel to form Fe_3O_4/bPEI nanocomposites. Although there have been some reports on the formation of Fe_3O_4 NPs by the reaction of Fe^{3+} and Fe^{2+} with $NH_3{\cdot}H_2O$ [43, 44], it might be the first observation that Fe_3O_4 NPs could be in-situ generated on the surface of nanogel to fabricate magnetic Fe_3O_4/bPEI nanocomposites for the purpose of easy separation. This method not only avoids the need of complex surface modification of Fe_3O_4 NPs, but also provides a new way to construct the magnetic polymeric nanocomposites.

The surface morphology of bPEI nanogel, Fe_3O_4/bPEI nanocomposites and the size distribution of Fe_3O_4 NPs were recorded by TEM, as shown in Fig. 3. It was found that bPEI nanogel displayed a well-defined spherical morphology with an average size of 183 ± 54 nm (Fig. 3a). As presented in Fig. 3b–e, it was clear that the Fe_3O_4 NPs assembled on the surface of bPEI nanogel, in consistent with the consequence of in-situ generation of Fe_3O_4, and their quantities gradually increased with the increase of the amount of Fe^{3+} and Fe^{2+} precursor solution used during the preparation process, as also proved by the FTIR and TGA results. It was obvious that $Fe_3O_{4(8)}$/bPEI contained the maximum amount of Fe_3O_4 NPs in Fe_3O_4/bPEI samples, together with some scattered Fe_3O_4 NPs, suggesting that the amount of Fe_3O_4 NPs exceeded the available spaces on the surface of bPEI nanogel (Fig. 3e).

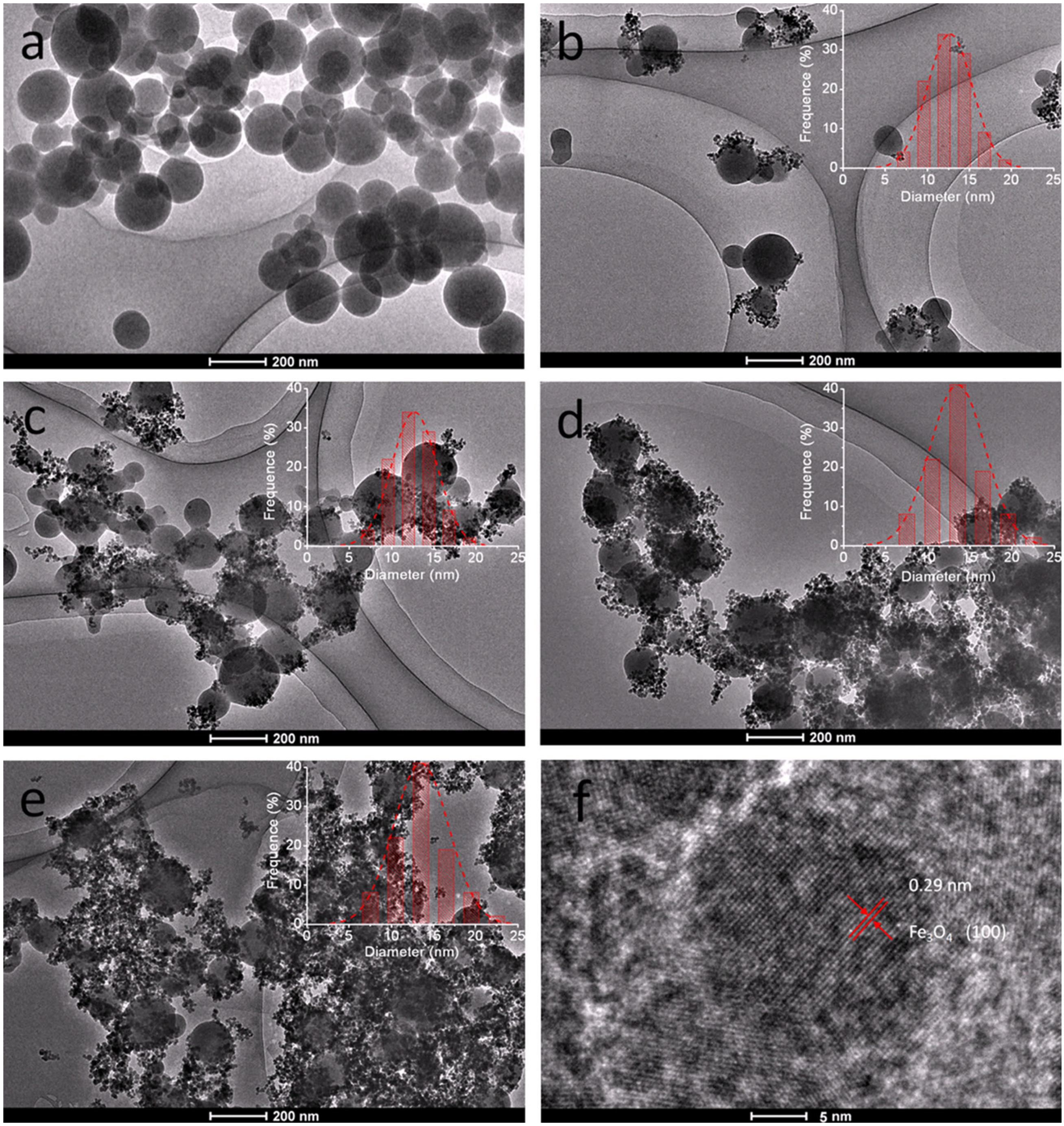

Fig. 3 TEM images of **a** bPEI nanogel, **b** $Fe_3O_{4(1)}$/bPEI, **c** $Fe_3O_{4(2)}$/bPEI, **d** $Fe_3O_{4(4)}$/bPEI, and **e** $Fe_3O_{4(8)}$/bPEI, and the size distribution of Fe_3O_4 (*inset*), **f** HRTEM image of $Fe_3O_{4(2)}$/bPEI

Notably, the average size and distribution of Fe_3O_4 NPs in all Fe_3O_4/bPEI samples was almost constant, approximately 13 nm in diameter, similar to those of the pure Fe_3O_4 (Fig. S4). As is well known, magnetite NPs with size below 25 nm (the critical size) present superparamagnetism [45]. Thus, these in-situ generated Fe_3O_4 NPs should present superparamagnetism, resulting in the superparamagnetism of the Fe_3O_4/bPEI nanocomposites and avoiding the disturbance from different contents of Fe_3O_4. Furthermore, the lattice of Fe_3O_4 phase can be observed in the high-resolution transmission electron microscopic (HRTEM) image of Fe_3O_4 NPs in $Fe_3O_{4(2)}$/bPEI (Fig. 3f). Its distance of 0.29 nm corresponded to the (100) crystal planes of the Fe_3O_4 phase [39].

Since the superparamagnetic properties of these materials are critical to ensure their applications, the magnetic properties of Fe_3O_4/bPEI nanocomposites were investigated and their magnetic hysteresis loops at room temperature are illustrated in Fig. 4. It should be noted that no remanence or hysteresis loops are detectable in all Fe_3O_4/bPEI samples, indicating their superparamagnetism [46], and in consistent with the expectation from the TEM results. The saturation magnetizations (*Ms*) values of the Fe_3O_4/bPEI nanocomposites were 53.2, 38.2, 28.7, 18.0 emu g^{-1} at an applied field of 20 000 Oe, respectively, all lower than that of pure Fe_3O_4 (71.5 emu g^{-1}). It is obvious that the *Ms* values of the Fe_3O_4/bPEI nanocomposites increased with the increase of the amount of Fe^{3+} and Fe^{2+} precursor solution used during the preparation process. Considering that $Fe_3O_{4(2)}$/bPEI can be separated within 6 s (inset of Fig. 4), the magnetism of these Fe_3O_4/bPEI nanocomposites should be strong enough for quick magnetic separation by an external magnetic field.

Dyes adsorption

Due to the nanosize effect and the high density of amine groups in the polymer network, the as-prepared Fe_3O_4/bPEI nanocomposites should have good capability on dyes adsorption. Thus, the adsorptions of CR (an anionic dye) and MB (a cationic dye) by the $Fe_3O_{4(2)}$/bPEI nanocomposite were then carried out to evaluate their adsorption capabilities. The chemical structures of the dyes and the digital photos of magnetic separation after dye absorptions are shown in Fig. 5. As can be seen, $Fe_3O_{4(2)}$/bPEI nanocomposite, containing moderate amount of Fe_3O_4, exhibited different adsorption behaviors toward different type of dyes. It can adsorb CR effectively and then be separated by an external magnetic field, whereas it cannot adsorb MB under similar conditions.

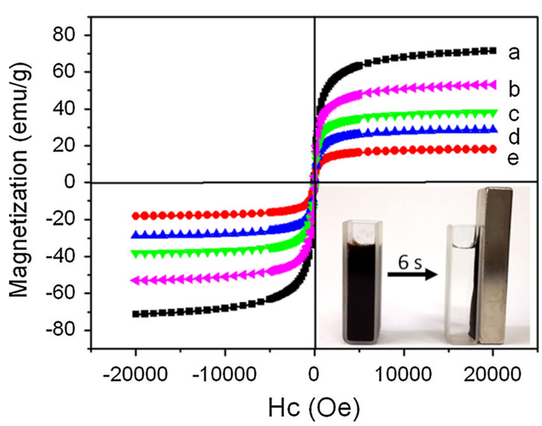

Fig. 4 Room temperature hysteresis loops of **a** pure Fe_3O_4, **b** $Fe_3O_{4(8)}$/bPEI, **c** $Fe_3O_{4(4)}$/bPEI **d** $Fe_3O_{4(2)}$/bPEI, and **e** $Fe_3O_{4(1)}$/bPEI. The inset photograph: separation of $Fe_3O_{4(2)}$/bPEI nanocomposite from aqueous dispersion by an external magnetic field

Subsequently, the effects of the Fe_3O_4 contents in the Fe_3O_4/bPEI nanocomposites and the pH values of the solution on their adsorption performance were systematically examined and the results are shown in Fig. 6. In the case of CR, the adsorption rate increased with the increase of the Fe_3O_4 contents in the Fe_3O_4/bPEI nanocomposites (Fig. 6a), and $Fe_3O_{4(8)}$/bPEI exhibited the maximal adsorption rate in the Fe_3O_4/bPEI samples studied in neutral medium (pH 7). This phenomenon can be explained by the gradually increased contents of Fe_3O_4, which also possessed certain adsorption capability toward CR, in these nanocomposites. Nevertheless, the adsorption ratios of all samples were up to about 98 % within 25 min, suggesting that the Fe_3O_4/bPEI nanocomposites could be served as high-efficiency adsorbents toward CR in neutral medium. In contrast, they showed almost no capability on the adsorption of MB.

On the other hand, $Fe_3O_{4(2)}$/bPEI exhibited different adsorption performances under different pH values (Fig. 6b). As can be seen, $Fe_3O_{4(2)}$/bPEI showed almost equal adsorption rates toward CR in alkaline medium (pH 10) and neutral medium (pH 7), both higher than that in acidic medium (pH 4). The charge interaction between CR (negative) and bPEI nanogel (positive) was believed to be beneficial for the high adsorption rate of $Fe_3O_{4(2)}$/bPEI in alkaline and neutral medium [22, 24]. However, the ionization of sodium sulfonate group in CR was inhibited in acidic medium, thus decreasing its interaction with nanogel and resulting in its lower adsorption rate. In contrast, $Fe_3O_{4(2)}$/bPEI showed quite low adsorption capability toward MB in acidic, neutral, or alkaline medium (Fig. 6b), and all adsorption ratios were still lower than 2.5 % even extending the adsorption time to 12 h. This phenomenon was mainly attributed to the electrostatic repulsion of positive charge between MB and bPEI nanogel [22, 24].

As inspired by the distinct adsorption efficiency toward CR and MB, the Fe_3O_4/bPEI nanocomposites should be used as selective adsorbents toward CR in the mixed-dye solution of CR and MB. As expected, $Fe_3O_{4(2)}$/bPEI can selectively adsorb CR in the aqueous mixture of CR and MB (Fig. 5d). As can be seen from the UV–vis spectra of mixed-dye solution after adsorption (Fig. S5), the absorption peak of CR almost disappeared, indicating the selective adsorption of CR. On the contrary, the absorption peak of MB was even higher than that before adsorption together with the increase of $A_{663} : A_{613}$, which was attributed to the disaggregation of MB dimer in the absence of CR [47]. Thus, these novel nanocomposites can be applied as high-efficiency adsorbents for CR, as well as selective adsorbents for the removal of CR from the aqueous mixture of

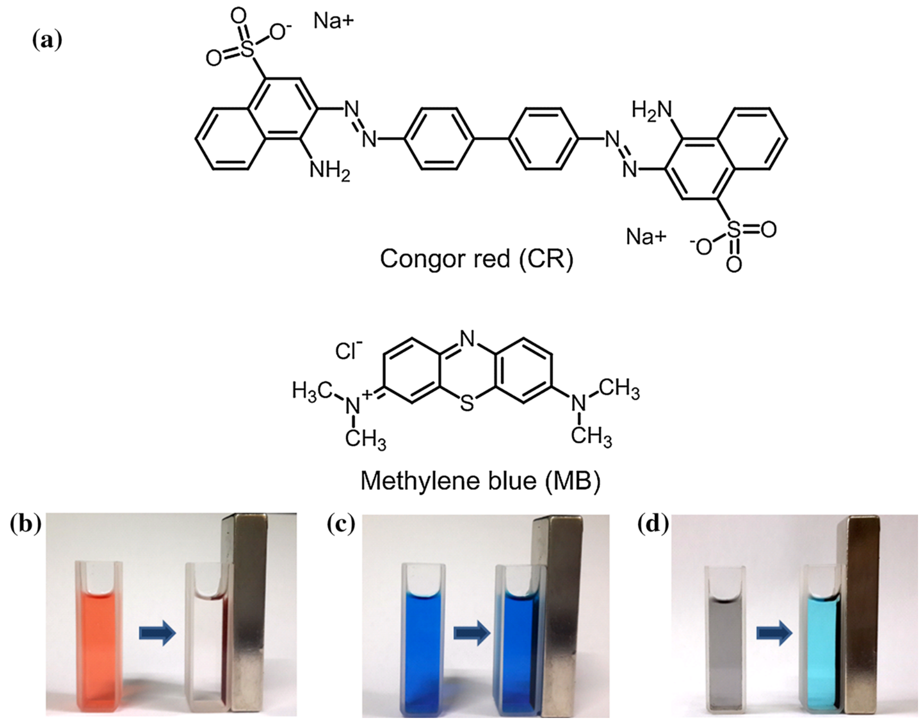

Fig. 5 **a** Chemical structures of CR and MB; and the digital photos of dye solution before and after absorptions by the $Fe_3O_{4(2)}$/bPEI nanocomposite, **b** 80 mg L^{-1} of CR, **c** 80 mg L^{-1} of MB, and **d** the mixture of CR (53.3 mg L^{-1}) and MB (26.7 mg L^{-1})

CR and MB, making them attractive candidates for dye adsorption.

Characterization and catalytic performance of Pd-$Fe_3O_{4(2)}$/bPEI

Owing to the numerous amine groups in bPEI, it has been applied as an excellent catalyst support of noble metal NPs to solve the agglomeration problems in many chemical reactions [48, 49]. Therefore, $Fe_3O_{4(2)}$/bPEI was chosen to act as the support of Pd NPs to prepare a novel Pd-$Fe_3O_{4(2)}$/bPEI catalyst. First, H_2PdCl_4 was absorbed by amine groups of $Fe_3O_{4(2)}$/bPEI at room temperature (Scheme 1). When excess $NaBH_4$ was used, the color of suspension changed from dark brown to black, indicating that H_2PdCl_4 was reduced to Pd(0) [50]. TEM image of Pd-$Fe_3O_{4(2)}$/bPEI is illustrated in Fig. 7a. As can be seen, the deposited Pd NPs were dispersed on the surface of $Fe_3O_{4(2)}$/bPEI with an average size of 2.74 $\pm$ 0.32 nm. Figure 7b shows a high-resolution TEM (HRTEM) micrograph that revealed the detailed lattice of Pd NPs in $Fe_3O_{4(2)}$/bPEI. The fringe spacing was approximately 0.22 nm, which corresponded to the (111) plane distance of the pure Pd (JCPDS: 89-4897). Furthermore, ICP-MS analysis showed that the Pd content in as-prepared Pd-$Fe_3O_{4(2)}$/bPEI was 2.60 wt% and the actual amount of Pd was 8.4 $\times$ 10^{-6} g in each experiment. In addition, the morphology of $Fe_3O_{4(2)}$/bPEI and crystallite phase of Fe_3O_4 was well-preserved during the preparation of Pd-$Fe_3O_{4(2)}$/bPEI (Figs. S6 and S7). However, no characteristic diffraction related to Pd was observed in XRD pattern of Pd-$Fe_3O_{4(2)}$/bPEI, probably due to its low content in the Pd-$Fe_3O_{4(2)}$/bPEI catalyst.

With this magnetic Pd-$Fe_3O_{4(2)}$/PEI catalyst in hand, the reduction of nitrophenols was chosen as the model reaction to evaluate its catalytic properties. In the presence of $NaBH_4$, the aqueous solutions of nitrophenols exhibited maximum adsorption peaks at 400 nm, 397 nm, and 413 nm, respectively (Fig. 8a, c, e). With the addition of Pd-$Fe_3O_{4(2)}$/bPEI, the absorbance at the maximum absorptions gradually decreased with prolonging the reaction time, indicating the reduction of nitrophenols, as also evidenced by the fading of yellow-green color of the reaction solution. All of these adsorption peaks disappeared within 190 s (Fig. S8), suggesting the completion of the reduction. In contrast, when $Fe_3O_{4(2)}$/bPEI was used instead of Pd-$Fe_3O_{4(2)}$/bPEI in these reductions under the same reaction conditions, there was no obvious decrease in the maximum absorptions, demonstrating that Pd is the key active species in Pd-$Fe_3O_{4(2)}$/bPEI for the reduction of nitrophenols.

As is well known, the apparent rate constant (k_{app}) was believed as an important parameter to quantitatively evaluate the catalytic activity of catalyst. Thus, k_{app} for the reduction of different nitrophenols over Pd-$Fe_3O_{4(2)}$/bPEI was calculated and compared. Considering that $NaBH_4$ was in a great excess throughout the reaction, its concentration could be considered as a constant. Therefore, the catalytic reduction of nitrophenols was simplified to be a pseudo-

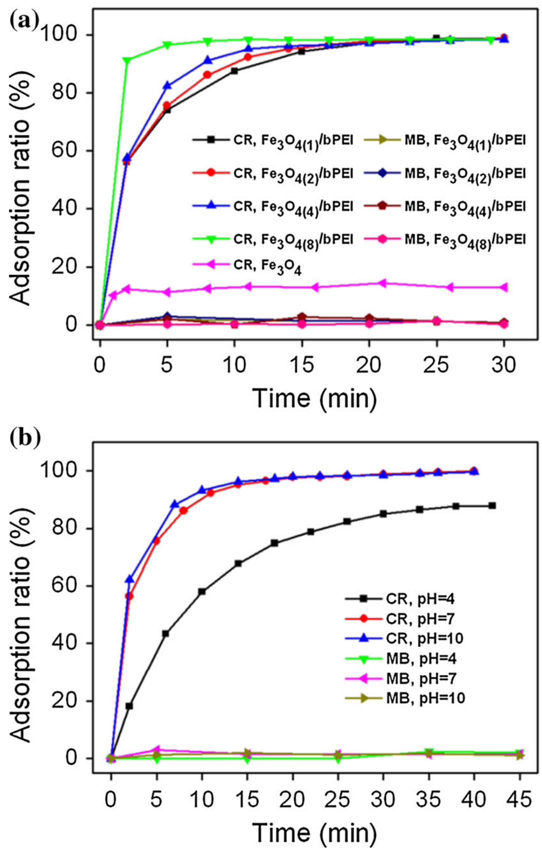

Fig. 6 **a** Adsorption curves of Fe_3O_4/bPEI nanocomposites toward CR and MB in neutral medium (pH 7). **b** Adsorption curves of $Fe_3O_{4(2)}$/bPEI nanocomposite toward CR and MB in different mediums

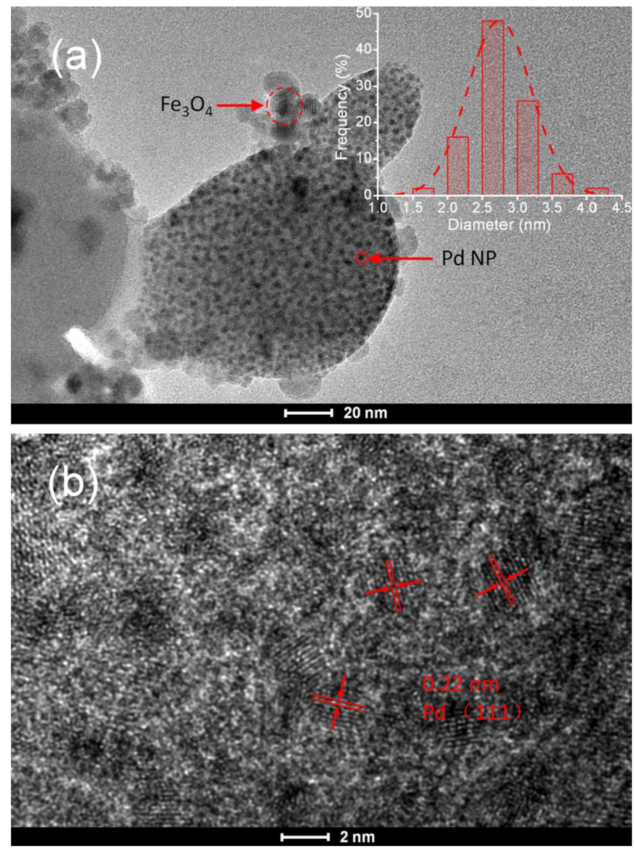

Fig. 7 **a** TEM image of Pd-$Fe_3O_{4(2)}$/bPEI and the size distribution of Pd (*inset*), **b** HRTEM image of Pd-$Fe_3O_{4(2)}$/bPEI

first-order kinetics reaction. Thus, k_{app} can be calculated based on the following equation: $\ln(A_t/A_0) = \ln(C_t/C_0) = -k_{app}t$, where A_t and C_t are the absorbance and concentration of nitrophenols at time t; A_0 and C_0 are the initial absorbance and concentration of nitrophenols, respectively. The linear relationships between $\ln(C_t/C_0)$ and the reaction time t are presented in Fig. 8b, d, and f. Therefore, the k_{app} of nitrophenols was calculated to be 0.0173, 0.0172, 0.0215 s^{-1}, respectively. It was found that the k_{app} followed the order of 4-NP > 2-NP > 3-NP, which was mainly attributed to the resonance structure and steric effect of the generated nitrophenolate ions, in agreement with the previous results [51–53]. Notably, there was no delay time observed in the initial period of those reductions. Since delay time was generally interpreted in terms of the time required for reactants to diffuse to the surface of the catalyst, this phenomenon illustrated that the Pd NPs were not in the polymer network of bPEI nanogel, but on the surface of $Fe_3O_{4(2)}$/bPEI, thus accounting for the good catalytic performance of Pd-$Fe_3O_{4(2)}$/bPEI. Furthermore, the k_{app} of the reduction of 4-NP was 0.0215 s^{-1}, which was higher than those of PAMAM-supported Pd NPs (0.006 s^{-1}) [54], spherical polyelectrolyte brushes and core–shell microgels supported-Pd NPs (0.0073 and 0.0025 s^{-1}) [55], magnetically recoverable Au nanocatalyst (0.0087 s^{-1}) [56] and PMMA-protected Au NPs (0.013 s^{-1}) [57], and polypyrrole-TiO_2 nanofibers-supported Pd nanocatalysts (0.0122 s^{-1}) [58], but was lower than those of amphiphilic bPEI-supported Pd NPs (0.045 s^{-1}) [59] and Pd NPs deposited on highly ordered mesoporous SBA (0.715 s^{-1}) [60].

It is well known that efficient recoverability and good reusability were both key points for an excellent catalyst. Thus, the recoverability and reusability of Pd-$Fe_3O_{4(2)}$/bPEI were evaluated using the reduction of 4-NP as a model reaction. As can be seen, Pd-$Fe_3O_{4(2)}$/bPEI can be easily separated by an external magnetic field (Fig. S8), and then be successfully cycled for ten successive runs in the reduction of 4-NP, with a conversion efficiency of about 99 % within 190 s (Fig. 9). This result was attributed to the use of $Fe_3O_{4(2)}$/bPEI as catalyst support, which can effectively inhibit the aggregation between the active Pd NPs, mainly due to the robust stabilizing effect of numerous amine groups on bPEI nanogel. Therefore, the as-prepared Fe_3O_4/bPEI was proven to be an excellent catalyst support of Pd NPs in the reduction of nitrophenols.

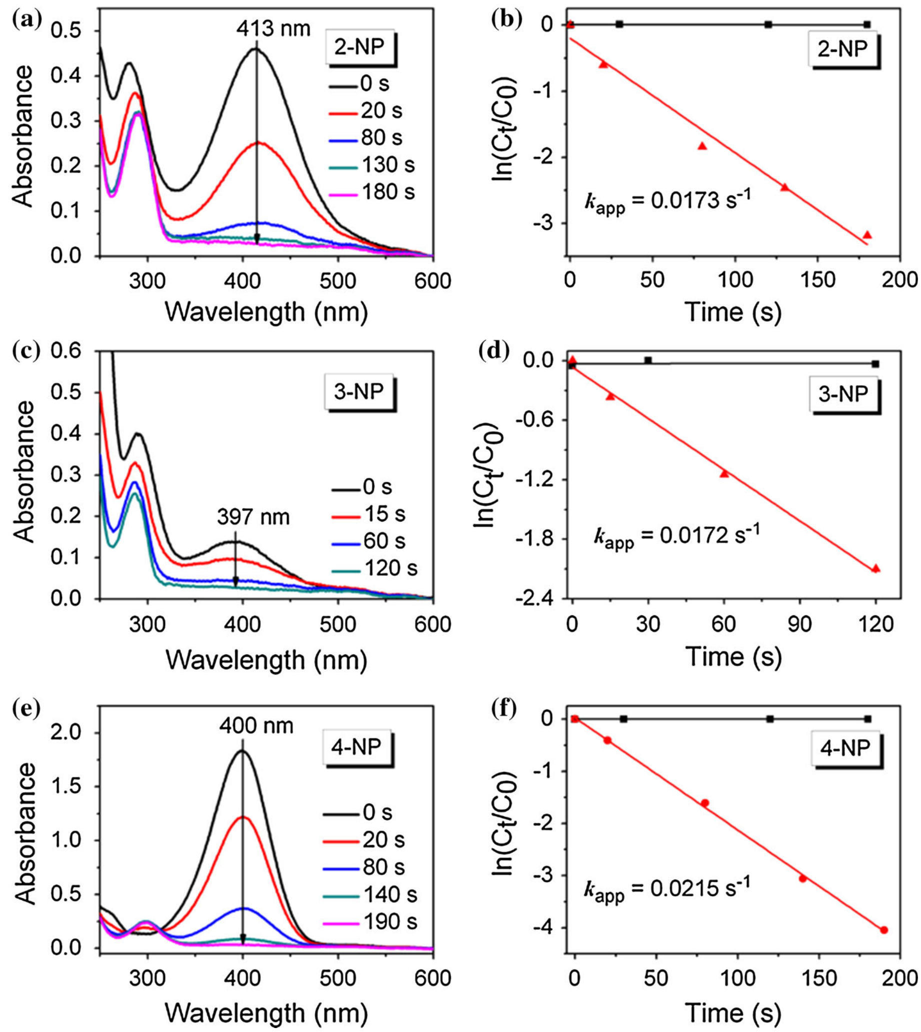

Fig. 8 Time-dependent UV–vis spectra (**a**, **c**, and **e**) and relationship between ln(C_t/C_0) and reaction time (**b**, **d** and **f**) on the reduction of nitrophenols (2-NP, 3-NP, and 4-NP) with $NaBH_4$ catalyzed by Pd-$Fe_3O_{4(2)}$/bPEI

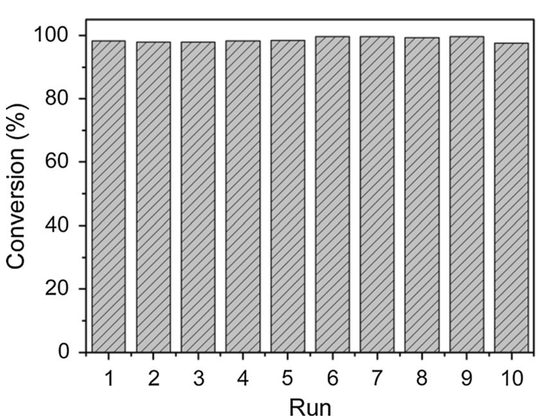

Fig. 9 Influence of cycle number on the conversion of 4-NP within 190 s

Conclusion

In summary, four novel magnetically recyclable Fe_3O_4/bPEI nanocomposites with in-situ generated Fe_3O_4 were successfully prepared via a facile approach in this work. Morphologies and magnetic properties of these Fe_3O_4/bPEI nanocomposites could be easily controlled by regulating the ratio between bPEI nanogel and Fe_3O_4 precursor. The in-situ generated Fe_3O_4 NPs endow these nanocomposites superior magnetic properties, making them easily separated by an external magnetic field. The as-prepared Fe_3O_4/bPEI nanocomposites could be used as efficient and selective adsorbents toward CR. Furthermore, they were also demonstrated to be excellent catalyst supports for Pd NPs. The obtained Pd-$Fe_3O_{4(2)}$/bPEI catalyst showed efficient reusability in the reduction of nitrophenols. Due to these advantages, the novel Fe_3O_4/bPEI nanocomposites can be applied as recyclable adsorbents toward anionic dyes and catalyst supports in various catalytic reactions. Particularly, this strategy with in-situ generation of Fe_3O_4 on bPEI nanogel provided a new approach for exploring magnetically driven recyclable polymeric nanocomposites.

Acknowledgements The authors thank Professor Gang Ma for his kind help. Financial support by the National Natural Science Foundation of China (21376060), the Natural Science Foundation of Hebei

Province (B2014201024), and the Youth Foundation of Hebei Educational Committee (QN2014069) is gratefully acknowledged.

References

1. Ryu JH, Jiwpanich S, Chacko R et al (2010) Surface-functionalizable polymer nanogels with facile hydrophobic guest encapsulation capabilities. J Am Chem Soc 132:8246–8247
2. Yuan Z, Wang Y, Chen D (2014) Preparation and characterization of thermo-, pH-, and magnetic-field-responsive organic/inorganic hybrid microgels based on poly (ethylene glycol). J Mater Sci 49:3287–3296. doi:10.1007/s10853-014-8037-2
3. Zhang X, Malhotra S, Molina M et al (2015) Micro-and nanogels with labile crosslinks–from synthesis to biomedical applications. Chem Soc Rev 44:1948–1973
4. Xiong Y, Wang H, Wang R et al (2010) A facile one-step synthesis to cross-linked polymeric nanoparticles as highly active and selective catalysts for cycloaddition of CO_2 to epoxides. Chem Commun 46:3399–3401
5. Moore BL, Moatsou D, Lu A et al (2014) Studying the activity of the MacMillan catalyst embedded within hydrophobic cross-linked polymeric nanostructures. Polym Chem 10:3487–3494
6. Li B, Jiang X, Yin J (2012) Multi-responsive microgel of hyperbranched poly(ether amine)(hPEA-mGel) for the selective adsorption and separation of hydrophilic fluorescein dyes. J Mater Chem 22:17976–17983
7. Bhardwaj P, Singh V, Mandal UK et al (2010) Polyacrylamide and poly (acrylamide-co-2-acrylamido-2-methyl-1-propanesulfonic acid)-silica composite nanogels through in situ microemulsion polymerisation. J Mater Sci 45:1008–1016. doi:10.1007/s10853-009-4032-4
8. Kaewsaneha C, Tangboriboonrat P, Polpanich D et al (2013) A. Janus colloidal particles: preparation, properties, and biomedical applications. ACS Appl Mater Interfaces 5:1857–1869
9. Sasaki Y, Akiyoshi K (2010) Nanogel engineering for new nanobiomaterials: from chaperoning engineering to biomedical applications. Chem Rec 10:366–376
10. Wu W, Mitra N, Yan EC et al (2010) Multifunctional hybrid nanogel for integration of optical glucose sensing and self-regulated insulin release at physiological pH. ACS Nano 4:4831–4839
11. Smith MH, Lyon LA (2011) Multifunctional nanogels for siRNA delivery. Acc Chem Res 45:985–993
12. Argentiere S, Blasi L, Morello G et al (2011) A novel pH-responsive nanogel for the controlled uptake and release of hydrophobic and cationic solutes. J Phys Chem C 115:16347–16353
13. Lu A, Moatsou D, Longbottom DA et al (2013) Tuning the catalytic activity of L-proline functionalized hydrophobic nanogel particles in water. Chem Sci 4:965–969
14. Bonomi P, Servant A, Resmini M (2012) Modulation of imprinting efficiency in nanogels with catalytic activity in the Kemp elimination. J Mol Recognit 25:352–360
15. Oishi M, Miyagawa N, Sakura T et al (2007) pH-responsive PEGylated nanogel containing platinum nanoparticles: application to on–off regulation of catalytic activity for reactive oxygen species. React Funct Polym 67:662–668
16. Pourjavadi A, Nazari-Chamazkoti M, Hosseini SH (2015) Polymeric ionic liquid nanogel-anchored tungstate anions: a robust catalytic system for oxidation of sulfides to sulfoxides. New J Chem 39:1348–1354
17. Sui ZY, Cui Y, Zhu JH et al (2013) Preparation of three-dimensional graphene oxide–polyethylenimine porous materials as dye and gas adsorbents. ACS Appl Mater Interfaces 5:9172–9179
18. Ma Y, Liu WJ, Zhang N et al (2014) Polyethylenimine modified biochar adsorbent for hexavalent chromium removal from the aqueous solution. Bioresource Technol 169:403–408
19. Heydari-Gorji A, Sayari A (2012) Thermal, oxidative, and CO_2-induced degradation of supported polyethylenimine adsorbents. Ind Eng Chem Res 51:6887–6894
20. Wang ML, Jiang TT, Lu Y et al (2013) Gold nanoparticles immobilized in hyperbranched polyethylenimine modified polyacrylonitrile fiber as highly efficient and recyclable heterogeneous catalysts for the reduction of 4-nitrophenol. J Mater Chem A 1:5923–5933
21. Zhang X, Zhang X, Yang B et al (2014) Biocompatible fluorescent organic nanoparticles derived from glucose and polyethylenimine. Colloid Surface B 123:747–752
22. Lupitskyy R, Minko S (2010) Robust synthesis of nanogel particles by an aggregation-crosslinking method. Soft Matter 6:4396–4402
23. Sun X, Yang L, Xing H et al (2013) Synthesis of polyethylenimine-functionalized poly(glycidyl methacrylate) magnetic microspheres and their excellent Cr(VI) ion removal properties. Chem Eng J 234:338–345
24. Fan Y, Liu HJ, Zhang Y et al (2015) Adsorption of anionic MO or cationic MB from MO/MB mixture using polyacrylonitrile fiber hydrothermally treated with hyperbranched polyethylenimine. J Hazard Mater 283:321–328
25. Lei Y, Chen F, Luo Y et al (2014) Three-dimensional magnetic graphene oxide foam/Fe_3O_4 nanocomposite as an efficient absorbent for Cr(VI) removal. J Mater Sci 49:4236–4245. doi:10.1007/s10853-014-8118-2
26. Xie Y, Yan B, Xu H et al (2014) Highly regenerable mussel-inspired Fe_3O_4@polydopamine-Ag core–shell microspheres as catalyst and adsorbent for methylene blue removal. ACS Appl Mater Interfaces 6:8845–8852
27. Mu B, Wang A (2015) One-pot fabrication of multifunctional superparamagnetic attapulgite/Fe_3O_4/polyaniline nanocomposites served as an adsorbent and catalyst support. J Mater Chem A 3:281–289
28. Mohammadi A, Barikani M, Barmar M (2013) Effect of surface modification of Fe_3O_4 nanoparticles on thermal and mechanical properties of magnetic polyurethane elastomer nanocomposites. J Mater Sci 48:7493–7502. doi:10.1007/s10853-013-7563-7
29. Xie W, Wang J (2014) Enzymatic production of biodiesel from soybean oil by using immobilized lipase on Fe_3O_4/poly(styrene-methacrylic acid) magnetic microsphere as a biocatalyst. Energy Fuel 28:2624–2631
30. Cai Y, Jiang JS, Zheng B et al (2013) Synthesis and properties of magnetic sensitive shape memory Fe_3O_4/poly(ε-caprolactone)-polyurethane nanocomposites. J Appl Polym Sci 127:49–56
31. Cui Q, Zhu S, Yan Y et al (2015) Superparamagnetic Fe_3O_4/poly(N-isopropyl acrylamide) nanocomposites synthesized in inverse miniemulsions: magnetic and particle properties. J Nanosci Nanotechnol 15:4608–4618
32. Zhao L, Liu H, Wang F et al (2014) Design of yolk–shell Fe_3O_4@PMAA composite microspheres for adsorption of metal ions and pH-controlled drug delivery. J Mater Chem A 2:7065–7074
33. Liu B, Zhang W, Yang F et al (2011) Facile method for synthesis of Fe_3O_4@polymer microspheres and their application as magnetic support for loading metal nanoparticles. J Phys Chem C 115:15875–15884
34. Guo W, Wang Q, Wang G et al (2013) Facile hydrogen-bond-assisted polymerization and immobilization method to synthesize hierarchical Fe_3O_4@poly(4-vinylpyridine-co-divinylbenzene)@Au nanostructures and their catalytic applications. Chem Asian J 8:1160–1167

35. Xuan S, Wang YXJ, Leung KCF et al (2008) Synthesis of Fe_3O_4@polyaniline core/shell microspheres with well-defined blackberry-like morphology. J Phys Chem C 112:18804–18809
36. Liu R, Guo Y, Odusote G et al (2013) Core–shell Fe_3O_4 polydopamine nanoparticles serve multipurpose as drug carrier, catalyst support and carbon adsorbent. ACS Appl Mater Interfaces 5:9167–9171
37. Tian Q, Wang Q, Yao KX et al (2014) Multifunctional polypyrrole@Fe_3O_4 nanoparticles for dual-modal imaging and in vivo photothermal cancer therapy. Small 10:1063–1068
38. Zhao M, Deng K, He L et al (2014) Core–shell palladium nanoparticle@metal–organic frameworks as multifunctional catalysts for cascade reactions. J Am Chem Soc 136:1738–1741
39. Xue Y, Chen H, Yu D et al (2011) Oxidizing metal ions with graphene oxide: the in situ formation of magnetic nanoparticles on self-reduced graphene sheets for multifunctional applications. Chem Commun 47:11689–11691
40. Yoon T, Chae C, Sun YK et al (2011) Bottom-up in situ formation of Fe_3O_4 nanocrystals in a porous carbon foam for lithium-ion battery anodes. J Mater Chem 21:17325–17330
41. Karami B, Hoseini SJ, Eskandari K et al (2012) Synthesis of xanthene derivatives by employing Fe_3O_4 nanoparticles as an effective and magnetically recoverable catalyst in water. Catal Sci Technol 2:331–338
42. Beyth N, Yudovin-Farber I, Bahir R et al (2006) Antibacterial activity of dental composites containing quaternary ammonium polyethylenimine nanoparticles against Streptococcus mutans. Biomaterials 27:3995–4002
43. Santoyo Salazar J, Perez L, de Abril O et al (2011) Magnetic iron oxide nanoparticles in 10–40 nm range: composition in terms of magnetite/maghemite ratio and effect on the magnetic properties. Chem Mater 23:1379–1386
44. Lee H, Lee E, Kim DK et al (2006) Antibiofouling polymer-coated superparamagnetic iron oxide nanoparticles as potential magnetic resonance contrast agents for in vivo cancer imaging. J Am Chem Soc 128:7383–7389
45. Liang J, Ma H, Luo W et al (2013) Synthesis of magnetite submicrospheres with tunable size and superparamagnetism by a facile polyol process. Mater Chem Phys 139:383–388
46. Zhang X, Jiang L (2011) Fabrication of novel rattle-type magnetic mesoporous carbon microspheres for removal of microcystins. J Mater Chem 21:10653–10657
47. Patil K, Pawar R, Talap P (2000) Self-aggregation of methylene blue in aqueous medium and aqueous solutions of Bu_4NBr and urea. Phys Chem Chem Phys 2:4313–4317
48. Ribeiro SM, Serra AC, Gonsalves ADAR (2011) Silica grafted polyethylenimine as heterogeneous catalyst for condensation reactions. Appl Catal A 399:126–133
49. Long W, Brunelli NA, Didas SA et al (2013) Aminopolymer–silica composite-supported Pd catalysts for selective hydrogenation of alkynes. ACS Catal 3:1700–1708
50. Yang J, Tian C, Wang L (2011) An effective strategy for small-sized and highly-dispersed palladium nanoparticles supported on graphene with excellent performance for formic acid oxidation. J Mater Chem 21:3384–3390
51. Wen X, Li G, Chen Q et al (2014) Organic-soluble palladium nanoparticles costabilized by hyperbranched polymer and dispersants as highly efficient and reusable catalysts in biphasic solution. Ind Eng Chem Res 53:11646–11652
52. Rashid M, Mandal TK (2008) Templateless synthesis of polygonal gold nanoparticles: an unsupported and reusable catalyst with superior activity. Adv Funct Mater 18:2261–2271
53. Li H, Gao S, Zheng Z et al (2011) Bifunctional composite prepared using layer-by-layer assembly of polyelectrolyte-gold nanoparticle films on Fe_3O_4-silica core-shell microspheres. Catal Sci Technol 1:1194–1201
54. Esumi K, Isono R, Yoshimura T (2004) Preparation of PAMAM − and PPI − metal (silver, platinum, and palladium) nanocomposites and their catalytic activities for reduction of 4-nitrophenol. Langmuir 20:237–243
55. Mei Y, Lu Y, Polzer F et al (2007) Catalytic activity of palladium nanoparticles encapsulated in spherical polyelectrolyte brushes and core-shell microgels. Chem Mater 19:1062–1069
56. Chang Y, Chen D (2009) Catalytic reduction of 4-nitrophenol by magnetically recoverable Au nanocatalyst. J Hazard Mater 165:664–669
57. Kuroda K, Ishida T, Haruta M (2009) Reduction of 4-nitrophenol to 4-aminophenol over Au nanoparticles deposited on PMMA. J Mol Catal A 298:7–11
58. Lu X, Bian X, Nie G et al (2012) Encapsulating conducting polypyrrole into electrospun TiO_2 nanofibers: a new kind of nanoreactor for in situ loading Pd nanocatalysts towards p-nitrophenol hydrogenation. J Mater Chem 22:12723–12730
59. Liu Y, Fan Y, Yuan Y et al (2012) Amphiphilic hyperbranched copolymers bearing a hyperbranched core and a dendritic shell as novel stabilizers rendering gold nanoparticles with an unprecedentedly long lifetime in the catalytic reduction of 4-nitrophenol. J Mater Chem 22:21173–21182
60. El-Sheikh SM, Ismail AA, Al-Sharab JF (2013) Catalytic reduction of *p*-nitrophenol over precious metals/highly ordered mesoporous silica. New J Chem 37:2399–2407